Optics Letters

Highly efficient cascaded amplification using Pr^{3+}-doped mid-infrared chalcogenide fiber amplifiers

Jonathan Hu,[1,*] Curtis R. Menyuk,[2] Chengli Wei,[1] L. Brandon Shaw,[3] Jasbinder S. Sanghera,[3] and Ishwar D. Aggarwal[4]

[1]Department of Electrical and Computer Engineering, Baylor University, One Bear Place #97356, Waco, Texas 76798, USA
[2]Department of Computer Science and Electrical Engineering, University of Maryland at Baltimore County, Baltimore, Maryland 21250, USA
[3]Naval Research Laboratory, Code 5620, Washington, DC 20375, USA
[4]Sotera Defense Solutions, 2200 Defense Highway, Crofton, Maryland 21114, USA
*Corresponding author: jonathan_hu@baylor.edu

Received 17 March 2015; revised 6 July 2015; accepted 16 July 2015; posted 16 July 2015 (Doc. ID 236293); published 3 August 2015

We computationally investigate cascaded amplification in a three-level mid-infrared (IR) Pr^{3+}-doped chalcogenide fiber amplifier. The overlap of the cross-sections in the transitions $^3H_6 \rightarrow {}^3H_5$ and $^3H_5 \rightarrow {}^3H_4$ enable both transitions to simultaneously amplify a single wavelength in the range between 4.25 μm and 4.55 μm. High gain and low noise are achieved simultaneously if the signal is at 4.5 μm. We show that 45% of pump power that is injected at 2 μm can be shifted to 4.5 μm. The efficiency of using a mid-IR fiber amplifier is higher than what can be achieved by using mid-IR supercontinuum generation, which has been estimated at 25%. This mid-IR fiber amplifier can be used in conjunction with quantum cascade lasers to obtain a tunable, high-power mid-IR source.

OCIS codes: (060.2390) Fiber optics, infrared; (160.5690) Rare-earth-doped materials; (230.2285) Fiber devices and optical amplifiers.

http://dx.doi.org/10.1364/OL.40.003687

Mid-infrared (IR) light sources are useful in many applications, such as biosensing, environmental monitoring, homeland security, and medical diagnostics [1]. Quantum cascade lasers are often used as light sources at mid-IR wavelengths [2–5]. Commercial tunable quantum cascade lasers are available with an average power that is typically in the range of 10–100 mW [6]. In order to obtain higher powers, a mid-IR amplifier is required.

In this Letter, we theoretically describe a cascaded amplifier that uses a Pr^{3+}-doped mid-IR amplifier, along with a pump at 2 μm, to achieve a slope efficiency of 45%. We will show that the threshold power is only 10 mW, so that when the pump power reaches 1–2 W, almost 45% of the pump power will be transferred into the 4–5-μm wavelength range.

For several applications, it is desirable to have a broadband source in the 4–5-μm range [7,8]. It is possible to use supercontinuum generation to directly transfer pump power from a source in the wavelength range between 2 and 3 μm to the wavelength range between 4 and 5 μm [9–11]. However, this approach can only transfer about 25% of the input power to the 3–5-μm wavelength range. A higher power source in the 4–5-μm wavelength range will lead to efficient supercontinuum generation, which will produce a broader spectrum [7].

The approach that we will propose is similar to the approach that has been used in earlier work to make rare-earth-doped fiber lasers and amplifiers [12–14]. Rare-earth ions Tb^{3+}, Dy^{3+}, and Pr^{3+} possess numerous transitions in the wavelength range from 3–12 μm and can be incorporated into chalcogenide glasses [15–19]. Theoretical studies showed that a three-level system using a Dy^{3+}-doped chalcogenide fiber can lase at 3.3 and 4.7 μm [14]. There are two separate lasing wavelengths because the emission spectra of the transition $^6H_{13/2} \rightarrow {}^6H_{15/2}$ (~3.3 μm) and the transition $^6H_{11/2} \rightarrow {}^6H_{13/2}$ (~4.7 μm) do not overlap. An idler at 3.3 μm is required to depopulate the ions in the excited level to obtain a slope efficiency of 16% in output power at a wavelength of 4.7 μm.

As in prior work [14], we are proposing to use a three-level system to provide gain. However, we are proposing to use transitions from the highest level (level 3) to the intermediate level (level 2) and from the intermediate level (level 2) to the lowest level (level 1), where the emission cross-sections of the two transitions overlap between 3.7 and 4.7 μm. As a consequence, both transitions can be simultaneously stimulated by a source at 4.5 μm, and the pump energy at 2 μm can be efficiently converted into energy at 4.5 μm. The rare-earth ion Tb^{3+}, like Dy^{3+}, does not have overlapping emission cross-sections in the wavelength range of interest; however, the rare-earth ion Pr^{3+} does have the required overlapping emission cross-sections.

We are thus proposing to use Pr^{3+}-doped chalcogenide fibers to amplify input light at 4.5 μm through the cascaded, two-transition process that we just described. Figure 1 shows

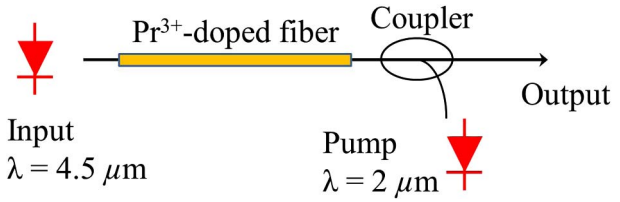

Fig. 1. Schematic illustration of the Pr^{3+}-doped chalcogenide fiber amplifier.

a schematic illustration of the Pr^{3+}-doped chalcogenide fiber amplifier. In Fig. 2, the blue solid curve and red dashed curve show, respectively, the emission cross-sections for the transitions $^3H_6 \rightarrow {}^3H_5$ (level 3 to level 2) and $^3H_5 \rightarrow {}^3H_4$ (level 2 to level 1) in a 1000-ppmw (parts per million by weight) Pr^{3+}-doped GeAsGaSe (GAGSe) sample [15–17]. The corresponding absorption cross-sections can be obtained using the McCumber relation [20–22]. We show the overlap between the two emission cross-sections in gray. Since this process is stimulated by light at 4.5 μm, one excited ion will radiate two photons that are coherent with light from the 4.5-μm source. This process is similar to the "two-for-one" cross-relaxation process in a Tm^{3+}-doped fiber amplifier, where an excited Tm^{3+} ion in $^3H_4$ (level 3) interacts with a ground state Tm^{3+} ion in $^3H_6$ (level 1) to produce two Tm^{3+} ions in the $^3F_4$ (level 2) laser level [23,24].

Figure 3 shows the energy diagram of the three lower levels of Pr^{3+} [15,16,25,26]. The higher levels are not included here because the transitions with the higher levels of $^3F_3$, $^3F_4$, and $^1G_4$ to the lower levels do not have a significant cross-section at the signal and pump wavelengths that we consider in this Letter. The rate equation for the three-level system can be written as [14,27]

$$\begin{aligned}\frac{dN_3}{dt} &= N_1 W_{a31} + N_2 W_{a32} - N_3(W_{e31} + W_{e32} + W_3),\\ \frac{dN_2}{dt} &= N_1 W_{a21} - N_2(W_{e21} + W_{a32} + W_{21}) \\ &\quad + N_3(W_{e32} + W_{32}),\\ N &= N_1 + N_2 + N_3, \end{aligned} \tag{1}$$

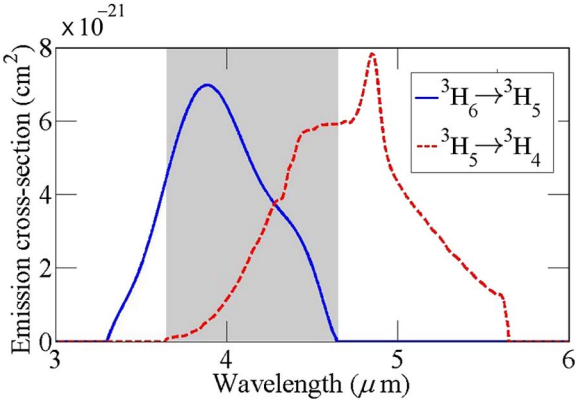

Fig. 2. Emission cross-sections in transition $^3H_6 \rightarrow {}^3H_5$ and $^3H_5 \rightarrow {}^3H_4$. Gray region shows the overlapped cross-section.

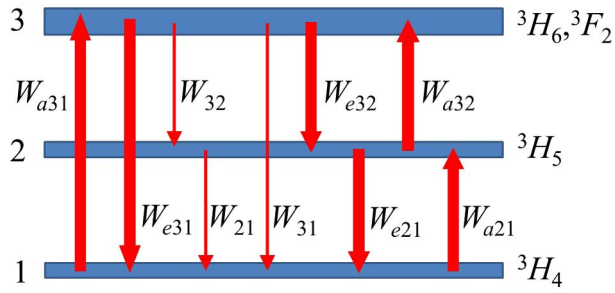

Fig. 3. Energy level diagram of Pr^{3+} with three lower levels.

where the subscripts a and e denote absorption and emission respectively, N_k is the number of ions in level k, $k = 1$–3, and N is the density of Pr^{3+}. We obtain the steady-state solution to Eq. (1) by setting $dN_k/dt = 0$, $k = 1$–3. Homogeneous broadening is used. The number of ions in one level is the same for different wavelengths. The transition probability per unit time between level i and level j that is denoted W_{ij} includes both spontaneous radiative and nonradiative decay [21,28]. The total spontaneous decay rate of level 3 is $W_3 = W_{32} + W_{31}$. The lifetime of level j is denoted $\tau_j = 1/W_j$. The branching ratio, $\beta_{32} = W_{32}\tau_3$, for the transition from level 3 to level 2 is used to obtain W_{32}. Stimulated rates are given by $W_{xij} = \Sigma P(\nu)\sigma_{xij}(\lambda)\Gamma(\nu)/Ah\nu$, where $x = a$ or e, $P(\nu)$ is the power, $\sigma_{xij}(\nu)$ is the cross-section corresponding to the particular transition (a or e) between levels i and j, $\Gamma(\nu)$ is the fractional overlap of the mode intensity with the ion-doped core, A is the core area, and Σ indicates the sum over all the frequencies or wavelengths. The gain per unit length for frequency ν is given by

$$\begin{aligned}\frac{dP(\nu)}{dz} &= [N_i(\nu)\sigma_{eij}(\nu) - N_j(\nu)\sigma_{aij}(\nu)]\Gamma(\nu)P(\nu)\\ &\quad + N_i\sigma_{eij}\Gamma(\nu)h\nu\Delta\nu - \alpha P(\nu), \end{aligned} \tag{2}$$

where the third and fourth terms on the right-hand side describe spontaneous emission [21,29] and fiber loss, respectively. The fiber loss is 1 dB/m [13,30]. We use a frequency step of $\Delta\nu = 12$ GHz in our simulations to resolve the amplified spontaneous emission (ASE) spectrum [29]. We have verified that the spectrum does not change when the frequency resolution is increased.

We obtain the fiber parameters for solving Eqs. 1 and 2 from Ref. [15]. The pump emission and absorption cross-sections between the levels of $^3H_6$ and $^3H_4$ are 1.6×10^{-21} cm^2 and 4.8×10^{-21} cm^2. Other parameters are $\beta_{32} = 0.42$, $\tau_3 = 2.7$ ms, and $\tau_2 = 12$ ms. The ion Pr^{3+} has a large absorption cross-section at 2 μm, which corresponds to the output spectra of, for example, Tm^{3+}- or Ho^{3+}-doped fiber lasers, which have output spectra of 1.8–2.1 μm [23]. In our simulations, we use an input wavelength of 1.95 μm with an input pump power of 10 W [31–33]. We set the Pr^{3+} ion density equal to 2×10^{19} cm^{-3}, which corresponds to 0.1 wt. % or 1000-ppmw Pr^{3+}-doped GeAsGaSe (GAGSe) glass fibers [15,17]. The equivalent atomic percentage of the Pr^{3+} is 0.055%. The cross-relaxation process is not considered in this Letter because of the low doping concentration [34,35]. We set

the core diameter and numerical aperture equal to 5 μm and 0.3, respectively, which are used to estimate the overlap factor $\Gamma(\nu)$ [21]. We simulate backward pumping, which has a higher slope efficiency than does forward pumping [36]. In the backward pumping scheme, the input signal powers are specified at one end of the fiber, and the input powers are specified at the other end. This two-point boundary-value problem is solved iteratively. To obtain convergence, we use a continuation method in which the pump power is gradually raised to its desired value [37]. ASE noise in both directions is included in our model for both the pump and the signal.

Figure 4 shows the gain as a function of fiber length at a signal wavelength of 4.5 μm. The maximum gain is 16 dB and 25 dB for an input power of 100 mW and 10 mW, respectively. The input power is assumed to be the power coupled input of the fiber regardless of any anti-reflection strategies. A slightly longer fiber must be used to obtain the maximum gain when the input signal power is reduced. With a fiber length less than 3 m, the fiber is not long enough to provide the maximum gain; with a fiber length greater than 5 m, the propagation losses increase for both the pump and the signal. Figure 5 shows the gain as a function of wavelength. The input signal power is 100 mW, and the fiber length is 3 m. The maximum gain is 16 dB at a wavelength of 4.5 μm. The amplifier gain is more than 10 dB in a broad spectrum of 300 nm between 4.25 μm and 4.55 μm. We also show the signal-to-noise ratio (SNR) in Fig. 5, which indicates that the maximum SNR occurs at a signal wavelength of 4.5 μm.

To explain the results in Fig. 5, we plot the output spectrum for input wavelengths of 4.0 μm, 4.5 μm, and 5.0 μm in Fig. 6. The input signal power and pump power are 100 mW and 10 W, respectively. We use a resolution bandwidth of 2 nm to plot the spectrum. When the input signal is at 5.0 μm, there is no light to depopulate the level $^3H_6$ (level 3), so that ASE noise due to the transition from level 3 to level 2 increases. When the input signal is at 4.0 μm, ASE noise due to the transition from level 2 to level 1 increases. However, when the signal is at 4.5 μm, the signal power can depopulate the ions in both level 3 and level 2 and be amplified by both the transition from level 3 to level 2 and the transition from level 2 to level 1. At the same time, ASE noise is suppressed.

We use slope efficiency to characterize how much of the pump power is converted to signal power [27]. Figure 7 shows the output signal power as a function of input pump power, which corresponds to a slope efficiency of around 45%. The input signal wavelength is 4.5 μm, and the input signal power is 100 mW. The inset shows the input pump power between 0 and 0.1 W, which indicates a threshold power of 10 mW. Figure 8 shows the slope efficiency when the input wavelength varies from 4 to 5 μm. The shape of the curve in Fig. 8 is consistent with the gain shape as a function of input wavelength, as shown in Fig. 5. The maximum slope efficiency is 45% at a

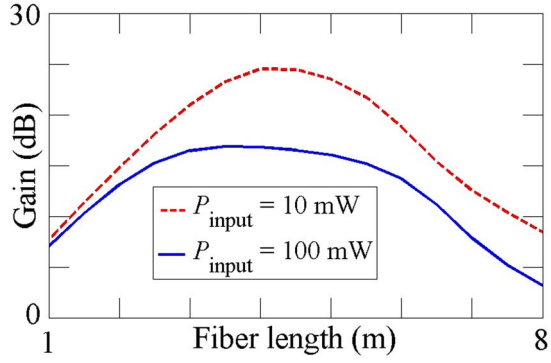

Fig. 4. Gain as a function of fiber length for input signal powers of 100 mW and 10 mW.

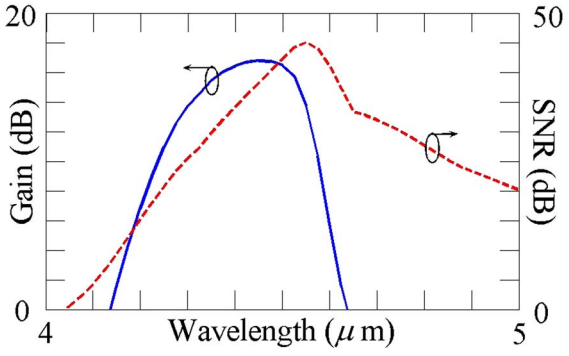

Fig. 5. Gain and SNR as a function of input signal wavelength.

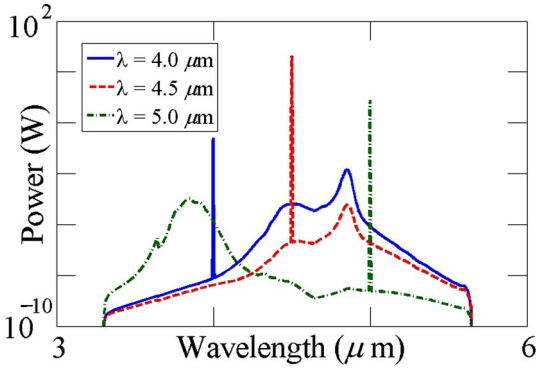

Fig. 6. Spectrum with different input wavelengths of 4.0, 4.5, and 5.0 μm.

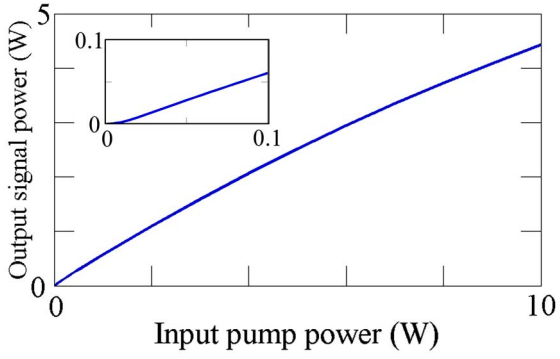

Fig. 7. Output signal power as a function of input pump power. The inset shows the input pump power between 0 and 0.1 W.

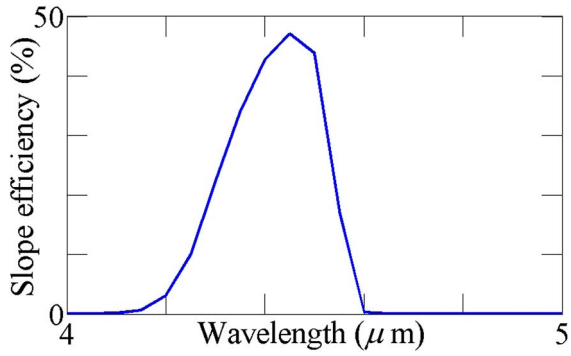

Fig. 8. Slope efficiency as a function of the input wavelength between 4 and 5 μm.

wavelength of 4.5 μm. This result shows that almost half of the input power at 2 μm can be converted to power at 4.5 μm when the input power is 1–2 W or higher. The efficiency of mid-IR generation using a fiber amplifier is thus higher than what can be obtained with direct supercontinuum generation with a pump at 2.0 μm, since 25% of the pump power can be transferred into the spectral range between 3 and 5 μm [30].

In summary, we show that maximum gains of 16 dB and 25 dB can be obtained using Pr^{3+}-doped chalcogenide fiber amplifiers at an input signal wavelength of 4.5 μm with input signal powers of 100 mW and 10 mW, respectively. The amplifier gain is more than 10 dB in a broad spectrum of 300 nm between 4.25 and 4.55 μm when the input signal power is 100 mW. High gain and low noise can be achieved simultaneously using the cascaded gain in three-level Pr^{3+}-doped fiber amplifiers. The slope efficiency is 45%, and the pump threshold is only 10 mW, so that almost half the pump power at 2 μm can be shifted to mid-IR light at 4.5 μm if pump lasers that produce 1–2 W or higher are used.

Funding. Vice Provost for Research at Baylor University; Naval Research Laboratory.

REFERENCES

1. A. Schliesser, N. Picqué, and T. W. Hänsch, Nat. Photonics **6**, 440 (2012).
2. Y. Yao, A. J. Hoffman, and C. F. Gmachl, Nat. Photonics **6**, 432 (2012).
3. R. F. Curl, F. Capasso, C. Gmachl, A. A. Kosterev, B. McManus, R. Lewicki, M. Pusharsky, G. Wysocki, and F. K. Tittel, Chem. Phys. Lett. **487**, 1 (2010).
4. J. Hu and C. Gmachl, Photon. Spectra **45**, 48 (2011).
5. J. Faist, F. Capasso, D. L. Sivco, C. Sirtori, A. L. Hutchinson, and A. Y. Cho, Science **264**, 553 (1994).
6. N. Anscombe, Electron. Opt. **210**, 16 (2011).
7. I. Kubat, C. S. Agger, U. Møller, A. B. Seddon, Z. Tang, S. Sujecki, T. M. Benson, D. Furniss, S. Lamrini, K. Scholle, P. Fuhrberg, B. Napier, M. Farries, J. Ward, P. M. Moselund, and O. Bang, Opt. Express **22**, 19169 (2014).
8. C. R. Petersen, U. Møller, I. Kubat, B. Zhou, S. Dupont, J. Ramsay, T. Benson, S. Sujecki, N. Abdel-Moneim, Z. Tang, D. Furniss, A. Seddon, and O. Bang, Nat. Photonics **8**, 830 (2014).
9. J. Hu, C. R. Menyuk, L. B. Shaw, J. S. Sanghera, and I. D. Aggarwal, Opt. Express **18**, 6722 (2010).
10. J. H. V. Price, T. M. Monro, H. Ebendorff-Heidepriem, F. Poletti, P. Horak, V. Finazzi, J. Y. Y. Leong, P. Petropoulos, J. C. Flanagan, G. Brambilla, X. Feng, and D. J. Richardson, IEEE J. Sel. Top. Quantum Electron. **13**, 738 (2007).
11. A. Marandi, C. W. Rudy, V. G. Plotnichenko, E. M. Dianov, K. L. Vodopyanov, and R. L. Byer, Opt. Express **20**, 24218 (2012).
12. B. J. Eggleton, B. Luther-Davies, and K. Richardson, Nat. Photonics **5**, 141 (2011).
13. J. S. Sanghera, L. B. Shaw, and I. D. Aggarwal, IEEE J. Sel. Top. Quantum Electron. **15**, 114 (2009).
14. R. S. Quimby, L. B. Shaw, J. S. Sanghera, and I. D. Aggarwal, IEEE Photon. Technol. Lett. **20**, 123 (2008).
15. L. B. Shaw, B. Cole, P. A. Thielen, J. S. Sanghera, and I. D. Aggarwal, IEEE J. Quantum Electron. **37**, 1127 (2001).
16. Ł. Sójka, Z. Tang, H. Zhu, E. Bereś-Pawlik, D. Furniss, A. B. Seddon, T. M. Benson, and S. Sujecki, Opt. Mater. Express **2**, 1632 (2012).
17. L. B. Shaw, B. B. Harbison, B. Cole, J. S. Sanghera, and I. D. Aggarwal, Opt. Express **1**, 87 (1997).
18. Z. Tang, D. Furniss, M. Fay, H. Sakr, L. Sójka, N. Neate, N. Weston, S. Sujecki, T. M. Benson, and A. B. Seddon, Opt. Mater. Express **5**, 870 (2015).
19. S. Sujecki, L. Sójka, E. Bereś-Pawlik, Z. Tang, D. Furniss, A. B. Seddon, and T. M. Benson, Opt. Quantum Electron. **42**, 69 (2010).
20. D. E. McCumber, Phys. Rev. **136**, A954 (1964).
21. P. C. Becker, N. A. Olsson, and J. R. Simpson, *Erbium-Doped Fiber Amplifiers Fundamentals and Technology* (Academic, 1999), Chap. 6.
22. R. S. Quimby, J. Appl. Phys. **92**, 180 (2002).
23. K. Scholle, S. Lamrini, P. Koopmann, and P. Fuhrberg, in *2 μm Laser Sources and Their Possible Applications*, B. Pal, ed., Frontiers in Guided Wave Optics and Optoelectronics (Intech, 2010), Chap. 21.
24. D. J. Richardson, J. Nilsson, and W. A. Clarkson, J. Opt. Soc. Am. B **27**, B63 (2010).
25. A. Oladeji, L. Sójka, Z. Tang, D. Furniss, A. Phillips, A. Seddon, T. Benson, and S. Sujecki, Opt. Quantum Electron. **46**, 593 (2014).
26. L. Sójka, Z. Tang, D. Furniss, H. Sakr, A. Oladeji, E. Bereś-Pawlik, H. Dantanarayana, E. Faber, A. B. Seddon, T. M. Benson, and S. Sujecki, Opt. Mater. **36**, 1076 (2014).
27. Y. Ohishi, T. Kanamori, Y. Terunuma, M. Shimizu, M. Yamada, and S. Sudo, IEEE Photon. Technol. Lett. **6**, 195 (1994).
28. Z. Burshtein, Opt. Eng. **49**, 091005 (2010).
29. C. R. Giles and E. Desurvire, J. Lightwave Technol. **9**, 271 (1991).
30. J. Hu, C. R. Menyuk, L. B. Shaw, J. S. Sanghera, and I. D. Aggarwal, Opt. Lett. **35**, 2907 (2010).
31. Q. Wang, J. Geng, T. Luo, and S. Jiang, Opt. Lett. **34**, 3616 (2009).
32. M. Eichhorn and S. D. Jackson, Appl. Phys. B **90**, 35 (2008).
33. M. Schellhorn, A. Hirth, and C. Kieleck, Opt. Lett. **28**, 1933 (2003).
34. T. Becker, R. Clausen, G. Huber, E. W. Duczynski, and P. Mitzscherlich, *Advanced Solid State Lasers Technical Digest* (Optical Society of America, 1989), paper DD1.
35. V. A. French, R. R. Petrin, R. C. Powell, and M. Kotka, Phys. Rev. B **46**, 8018 (1992).
36. X. Zhu and R. Jain, Appl. Opt. **45**, 7118 (2006).
37. J. Hu, B. S. Marks, Q. Zhang, and C. R. Menyuk, J. Opt. Soc. Am. B **22**, 2083 (2005).